Biomolecules and Biomedicine

ISSN: 2831-0896 (Print) | ISSN: 2831-090X (Online)

Journal Impact Factor® (2023): 3.1

CiteScore® (2023): 7.4

www.biomolbiomed.com | www.blog.bjbms.org

RESEARCH ARTICLE

Shi et al: ST6GAL1 and LGALS3BP sialylation in colorectal cancer

Multi-omics reveals that ST6GAL1 promotes colorectal cancer progression through LGALS3BP sialylation

Yuanchao Shi[1, 2], Zhenzhong Pan[3], Jingwei Duan[4], Zexing Wang[5], Yiliang Fang[6], Bo Tang[7*], Quanlin Guan[1, 2*]

[1]The First Clinical Academy of Lanzhou University, Lanzhou University, Lanzhou, China

[2]Department of General Surgery and Gastrointestinal Oncology Surgery, Lanzhou University First Hospital, Lanzhou, China

[3]State Key Laboratory of Biotherapy and Cancer Center, West China Hospital, Sichuan University, Chengdu, China

[4]Emergency department, Peking University Third Hospital, Beijing, China

[5]School of Medicine, Chongqing University, Chongqing, China

[6]Department of Neurology, Army Medical University Xinqiao Hospital, Chongqing, China

[7]Department of General Surgery and Center of Minimal Invasive Gastrointestinal Surgery, Third Military Medical University Southwest Hospital, Chongqing, China

*Correspondence to Quanlin Guan: guanql@lzu.edu.cn and Bo Tang: tangbo@sina.com

DOI: https://doi.org/10.17305/bb.2025.11663

ABSTRACT

ST6 β-galactoside α2,6-sialyltransferase 1 (ST6GAL1), a crucial enzyme for tumor-associated sialic acid modification, has been reported to positively correlate with colorectal cancer (CRC) tumorigenesis; however, the underlying mechanism remains unclear. To elucidate the protumor mechanisms of ST6GAL1, we performed transcriptomic and N-glycoproteomic analyses and in vitro assays. We found that ST6GAL1 was significantly upregulated in tumor samples than in matched normal samples by analyzing fresh clinical samples from public databases (mean mRNA expression level: tumor vs. normal samples = 0.002712:0.000966, $P < 0.05$, $n = 22$). The in vitro results revealed that ST6GAL1 overexpression promoted CRC cell proliferation, migration, and chemoresistance, which were significantly blocked by its knockdown. Transcriptomic data showed that many genes related to the four modules (proliferation/cell cycle, migration, motility, and epithelial-mesenchymal transition) were upregulated after ST6GAL1 overexpression but downregulated after ST6GAL1 knockdown. Furthermore, the N-glycoproteome data revealed that 25 substrates that were sialylated upon ST6GAL1 overexpression were related to protumor activity. Importantly, we found that knockdown of lectin galactoside-binding soluble 3-binding protein (LGALS3BP), a newly identified secreted substrate of ST6GAL1, significantly blocked the proliferation, invasion, and chemoresistance of CRC cells induced by ST6GAL1 overexpression. Treatment with sialidases (neuraminidases, NAs) also blocked the protumor activity of ST6GAL1. Thus, ST6GAL1-induced increased sialylation of substrates such as LGALS3BP and upregulation of protumor genes promote CRC tumorigenesis and chemoresistance, which provides important perspectives and new targets for the treatment of CRC.

Keywords: Colorectal cancer; CRC; ST6 β-galactoside α2,6-sialyltransferase; ST6GAL1; lectin galactoside-binding soluble 3-binding protein; LGALS3BP; sialylation

INTRODUCTION

Colorectal cancer (CRC) is a costliest malignant tumor that ranks second in terms of mortality and third in incidence among malignant tumors (1). While significant progress has been made

in the diagnosis and treatment of CRC, the incidence and mortality rates continued to increase in low- and middle-income countries (1) and have risen rapidly among younger adults (aged <55 years) since the mid-1990s (2, 3). Therefore, the molecular signatures of CRC tumorigenesis should be explored.

Sialylation is a common post-translational modification (PTM) that increases the diversity of proteins, lipids, and RNA. It is a biologically important form of glycosylation that is involved in embryonic development, neurodevelopment, reprogramming, and immune responses (4). Abnormal sialylation is associated with malignant transformation (5), and several sialylated glycoproteins such as prostate-specific antigen (PSA), cancer antigen 125 (CA125), and thyroglobulin (6) are used as clinical cancer biomarkers. Moreover, sialylation modifications such as those in epithelial-mesenchymal transition (EMT) (7, 8), malignant proliferation (9), migration (9), invasion (9), anti-apoptosis (10-12), cancer cell stemness (13, 14) and treatment resistance (15, 16) are widely involved in the process of tumor development. However, only few sialic-acid-modified molecules have been reported. Therefore, the identification of new sialylation substrates and elucidation of the detailed mechanisms of sialylation in tumorigenesis have gained attention.

Sialic acid is covalently attached to the underlying glycan chain via distinct glycosidic linkages (α2,3, α2,6, or α2,8) catalyzed by sialyltransferases (9). Abnormal sialylation mainly results from the altered expression of sialyltransferases. ST6 β-galactoside α2,6-sialyltransferase 1 (ST6GAL1) is the only enzyme that can synthesize α2,6-sialylated lactosamine (Sia6LacNAc) through the addition of α2,6-linked sialic acid to Galβ1,4GlcNAc (lactosamine) chains (17). Notably, high ST6GAL1 expression and increased sialylation have been reported in numerous cancer types, including pancreatic, colorectal, prostate, breast, and ovarian cancers (10, 18). Moreover, many studies have shown that ST6GAL1 correlates with high tumor grade, metastasis, and poor prognosis (9, 18). However, the mechanism through which ST6GAL1 promotes tumorigenicity is unclear. ST6GAL1 has been shown to induce EMT in pancreatic cancer cells and mediate chemoresistance through sialylation of epidermal growth factor receptor (9, 19). Moreover, sialylation of tumor necrosis factor receptor 1, Fas (CD95), and galectin-3 by ST6GAL1 conferred protection against apoptosis in cancer cells (10-12). Additionally, accumulation of over-sialylated lysosome-associated membrane protein 1 (LAMP1) exacerbates the lysosomal exocytosis of soluble hydrolases and exosomes from tumor cells, which can promote cancer cell invasion and metastasis (20). ST6GAL1 influences cancer progression not only through the direct sialylation of some substrates but also by

exerting effects other than PTMs. ST6GAL1 promoted TGF-β-dependent EMT in GE11 cells and maintained the mesenchymal state via growth signaling (7). ST6GAL1 protects tumor cells against hypoxic stress by augmenting the accumulation of hypoxia-inducible factor 1 subunit α in ovarian and pancreatic cancer cells (21). Furthermore, ST6GAL1 upregulation in ovarian and pancreatic carcinomas induced the expression of SRY-box transcription factor 9 and Snail family transcriptional repressor 2, which are key tumor-promoting transcription factors (14). These findings suggest that ST6GAL1 also regulates cancer cell progression through interactions with signaling networks.

The present study aimed to comprehensively investigate the role of ST6GAL1 and identify key sialylation substrates in CRC. We conducted transcriptomic and proteomic analyses and found that four module genes related to tumor progression were upregulated following ST6GAL1 overexpression. We performed modification omics on CRC cell lines to screen for sialic-modified substrates and identified galectin-3 binding protein (aka mac-2 BP, 90k, LGALS3BP) as a new sialylation molecule. LGALS3BP is highly expressed in tumors and is associated with poor clinical outcomes (22). However, the detailed underlying regulatory mechanisms remain unclear. Therefore, the mechanisms through which ST6GAL1 influences CRC progression should be investigated.

MATERIALS AND METHODS

Clinical samples

Twenty-two patients enrolled in the study were admitted to at the First Affiliated Hospital of the Army Medical University, PLA and were pathologically diagnosed with colorectal cancer. And underwent surgery at this hospital. The clinical samples used in this study were obtained from these patients during the operation. Fresh samples were transported to the laboratory within 30 min. Detailed clinical characteristics are summarized in Supplementary Table 1.

Cell culture

The human CRC cell lines HCT-116, HT-29, Caco2, SW48, and HEK293T were purchased from the American Type Culture Collection (Rockville, MD, USA). All cell lines were maintained in Dulbecco's modified Eagle's medium (DMEM; 6123081; Thermo Fisher Scientific, MA, USA) supplemented with 10% fetal bovine serum (FBS; 2535493P; Invitrogen, MA, USA) and 1% penicillin-streptomycin (2441886; Thermo Fisher Scientific). All cell lines were incubated in a humidified chamber with 5% CO_2 at 37 °C. All experiments were

performed using mycoplasma-free cells. The cells used in this study were identified via short tandem repeat profiling.

Cell line construction

To obtain cells stably transfected with ST6GAL1, the ST6GAL1 sequence was cloned into the pCDH-CMV-MCS-EF1-copGFP lentiviral vector. HEK293T cells were transfected with psPAX2, pMD2.G, or the lentiviral constructs. Supernatants were collected 48 h post transfection. After passing through 0.45 μm filters, viruses were used to infect target cells supplemented with 2 μg/mL polybrene. Subsequently, GFP^+ cells were sorted via flow cytometry. For ST6AGL1 and LGALS3BP knockdown, small hairpin RNAs targeting ST6GAL1 (CCCAGAAGAGATTCAGCCAAA) or LGALS3BP (GTACTTCTACTCCCGAAGGAT) were cloned into the plko.1-copGFP-PURO or plko.1-Hygro plasmid, respectively. HEK293T cells were transfected with psPAX2, pMD2.G, or the lentiviral constructs. After viral infection, positive cells were selected using 2 μg/mL puromycin and 100 μg/mL Hygromycin B, respectively. *ST6GAL1* expression was confirmed via reverse transcription quantitative polymerase chain reaction (RT-qPCR) and western blotting (WB).

Flow cytometry

The collected samples were fully chopped and digested with enzymes (1.5 mg/mL collagenase IV [11088866001; Roche, Basel, Switzerland], 1 mg/mL DNase I [10104159001, Roche], and 0.2 mg/mL dispase II [4942078001; Roche]) in basic DMEM at 37 °C for 30 min. The dissociated cells were passed through a 70 μm cell strainer and centrifuged. After washing with PBS (10010023; Thermo Fisher Scientific), the cells were resuspended in buffer (PBS supplemented with 1% FBS and 0.1% ethylenediaminetetraacetic acid).

For Sambucus nigra lectin (SNA) staining, the cells were incubated with 20 μg/mL SNA-FITC antibody (FL-1301-2; Vector Laboratories, CA, USA), PE-Cy7 mouse anti-human CD45 antibody (1:200, 557847; Biolegend, CA, USA), and eBioscience™ Fixable Viability Dye eFluor™ 780 (1:400, 65-0865-14; eBioscience, CA, USA) and analyzed via flow cytometry.

For the detection of tumor cell apoptosis, the cells were incubated with PE-conjugated Annexin V (AV, 1:200; 556422; BD, NJ, USA) in a buffer containing 7-amino-actinomycin (7-AAD, 1:200; 559925; BD) and analyzed via flow cytometry.

Colony formation and methyl thiazolyl tetrazolium (MTT) assay

For the colony formation assay, we seeded 250, 500, and 1,000 cells in each well of a six-well plate and replaced the culture medium after an average of 4 d. The number of clones formed was counted after 14 d.

For the cell viability assay, we seeded 8,000 cells in each well of a 96-well plate. The optical density values of different wells were measured at different time points using the MTT Cell Proliferation and Cytotoxicity Assay Kit (C009S; Beyotime, Shanghai, China) following the manufacturer's protocol.

Scratch assay and cell migration

A total of 1×10^6 cells were incubated overnight in six-well plates, and straight lines were lightly drawn. The cells were subsequently cultured in DMEM, 1% FBS, and 2% penicillin-streptomycin for different durations. Cell migration to the central scratch area were observed at each time point (days 0, 2, and 4).

Total RNA isolation and quantitative reverse transcription polymerase chain reaction

Total tissue RNA was extracted using the FastPure Cell/Tissue Total RNA Isolation Kit V2 (RC112-01; Vazyme, Nanjing, China) according to the manufacturer's instructions and reverse transcribed into cDNA using the PrimeScript™ RT Reagent Kit with gDNA Eraser (RR047A; TaKaRa Bio, Shiga, Japan). RT-qPCR was performed using the QuantiTect SYBR Green PCR Kit (1725121; Bio-Rad Laboratories, CA, USA). The primers used were designed by Beijing Tsingke Biotech Co., Ltd., and are listed in Supplementary Table 2. A. Gene expression levels were quantified using the $2^{-\Delta\Delta}$Ct method. Relative gene expression levels were obtained via sequential normalization of the values against those of GAPDH and the experimental controls.

WB

The cell pellet was lysed using radioimmunoprecipitation assay (RIPA) buffer (P0013C; Beyotime) supplemented with (phenylmethylsulfonyl fluoride; PMSF; ST507; Beyotime) and phosphatase inhibitors (P1081; Beyotime). Total protein concentration was determined using a bicinchoninic acid (BCA) assay (P0012S; Beyotime). Antibodies were used to measure the protein levels: ST6GAL1 (1:200, AF5924; R&D Systems, MN, USA), hGalectin-3BP (0.2 μg/mL, AF2226; R&D Systems), anti-GAPDH (1:3,000, 2118; Cell Signaling Technology, MA, USA), horseradish peroxidase-conjugated anti-goat secondary antibodies (1:2000, A0208; Beyotime), SNA (1:400, B-2; Vector Laboratories), SABC (A: B=1:1, 7074l; Beyotime). The blots were developed using BeyoECL (P0018S; Beyotime). Densitometry was performed using Fiji (ImageJ; National Institute of Health).

Hematoxylin & eosin (HE) and immunohistochemistry (IHC) Staining

The samples were fixed in 4% paraformaldehyde for 48 h. Dehydration and paraffin embedding were performed using routine methods. Paraffin-embedded tissue sections were stained with antibodies against ST6GAL1 (AF5924; R&D Systems) or B72.3 (915206; BioLegend). Staining was visualized using the Dako REAL^{TM} EnVision^{TM} Detection System (K5007; Dako, Denmark). The cell nuclei were re-stained with hematoxylin (C0105S; Beyotime) and differentiated with an acid-alcohol fast differentiation solution (C0163S; Beyotime). The slides were directly stained with hematoxylin, hydrochloric alcohol, and eosin.

Immunofluorescence (IFC) staining

Cells were fixed in 1% paraformaldehyde, permeabilized with 0.2% Triton X-100, blocked in 5% BSA, and then incubated with corresponding antibodies (SNA-FITC, 1:200; Alpha Diagnostic International, TX, USA; SNA15-FITC; SNA-HRP, 1:100; Alpha Diagnostic International; SNA15-HRP; hGalectin-3BP, 0.2 μg/mL; AF2226; R&D Systems). The sections were sealed with an antifade mounting medium supplemented with DAPI (P0131; Beyotime).

The Cancer Genome Atlas (TCGA) data analysis

TCGA colon adenocarcinoma (COAD) and rectal adenocarcinoma (READ) data were used. We calculated the average expression of ST6GAL1 after z-score normalization using the log-transformed expression profiles. Student's *t*-test was used to determine statistical significance. A Kaplan-Meier plotter was used to analyze the effects of genes on survival using RNA-sequencing (RNA-seq) data from TCGA, European Genome-phenome Archive, and Gene Expression Omnibus databases in patients with CRC, which were determined based on hazard ratios (HRs) with corresponding 95% confidence intervals and log-rank *P* values.

Bulk RNA-seq and analysis

Libraries were constructed using the NEBNext Poly (A) mRNA Magnetic Isolation Module Kit (New England Biolabs, MA, USA) and the NEBNext Ultra RNA Library Prep Kit for the Illumina paired-end Multiplexed Sequencing Library (New England Biolabs). The remaining qualified reads were aligned to the GRCm38 genome assembly using STAR (version 2.7.10a). The quantitative tool used was the RSEM, which generates a count table. The resulting matrix was transformed for downstream analyses. For differential expression analysis and pathway analysis, genes with *P*-adjusted < 0.05 and log2-fold change > 1 or < -1 were selected.

Proteomics and glycosylation omics

The samples were lysed (RIPA with 1% PMSF and 1% phosphatase inhibitor) and sonicated thrice on ice using a high-intensity ultrasonic processor (Scientz, China), and protein

concentration was determined using a BCA kit following the manufacturer's instructions. The sample was incubated with TCA, washed with precooled acetone, redissolved in tetraethylammonium bromide, ultrasonically dispersed, and trypsinized. The sample was subsequently reduced with 5 mM dithiothreitol for 60 min at 37 °C and alkylated with 11 mM iodoacetamide for 45 min at room temperature in the dark. Finally, the peptides were desalted and obtained using a C18 SPE column. Some protein samples were directly subjected to mass spectrometry and data processing, whereas others were subjected to biomaterial-based PTM enrichment (of N-glycopeptides). The eluted glycopeptides were desalted using C18 Zip Tips following the manufacturer's instructions and dried for MS analysis.

Data analysis of protein and glycosylations via omics

The resulting MS/MS data were processed using the MaxQuant search engine (v.1.6.15.0). To obtain high-quality results, the false discovery rate accuracy of the results at the three levels of spectrum, peptide, and protein after further data filtering was set to 1%. The identified proteins contained at least one specific peptide segment, and the segments and proteins were counted. The WolF PSORT software was used to predict subcellular localization for protein annotation and differential protein proportions. Additionally, we combined SW48-empty virus (EV) and SW48-OE bulk RNA-seq results. For the modification omics data combined with the quantitative omics results, we excluded differential expression caused by the deregulation of protein expression. N-glycosylation sites were verified using UniProt for annotations, and other annotations were predicted based on the sequence context using the NetNGlyc algorithm. We used the ratio of the relative quantitative value of each complete glycopeptide in the sample as the difference multiple and used a difference in expression > 1.5 as the significantly upregulated change threshold and < 1/1.5, as the significantly downregulated change threshold for differential complete glycopeptide screening. Gene ontology (GO) functional enrichment analysis was performed, and Fisher's exact test was used to analyze the significance of GO enrichment. Cluster analysis based on the functional enrichment of proteins corresponding to five different sugar types was used to investigate potential associations and differences in specific functions (GO, Kyoto Encyclopedia of Genes and Genomes pathway, protein domain, Reactome, and Wiki pathways). Statistical significance was set at $P < 0.05$.

Ethical statement

This study was approved by the Ethical Committee of the First Affiliated Hospital of the Army Medical University, PLA, and complied with all relevant ethical regulations. This

study was approved by the Ethical Committee of the First Affiliated Hospital of Army Medical University, PLA (No. (A) KY2022142). All patients signed informed consent forms prior to enrollment and sample collection.

Statistical analysis

All statistical analyses were performed using GraphPad Prism version 9 (GraphPad Software, USA) and SPSS version 25.0 (IBM Corp., Armonk, NY, USA) for Windows (Microsoft Corp., Redmond, WA, USA). We used Shapiro-Wilk test, combined with visual inspection, to confirm the normality of continuous variables, and all continuous variables conformed to normal distribution. Continuous variables were analyzed using Student's *t*-test and are expressed as the mean±standard deviation (SD). Pearson's correlation coefficient was used to analyze the association of ST6GAL1 mRNA with Ki-67 and Spearman's rank correlation was used to analyze the correlation between ST6GAL1 mRNA and clinical stage in patients. Statistical significance was set at $P < 0.05$.

RESULTS

ST6GAL1 upregulation positively correlates with the clinical stage of CRC

We investigated the ST6GAL1 expression level and its correlation with the α-2,6-sialylation level in CRC using TCGA data and found that ST6GAL1 expression was significantly higher in CRC tissues than in normal tissues (Figure 1A). To validate this, we analyzed twenty-two tumor and twenty-two paired adjacent normal samples from patients with CRC (clinical information shown in Supplementary Table S1). Although the expression levels were scattered in both groups, the ST6GAL1 transcriptional level was upregulated in twenty out of twenty-two paired tumor samples compared with adjacent normal samples (Figure 1B). Similarly, ST6GAL1 protein expression was higher in tumor samples (Figure 1C). We examined the correlation of the transcription level of ST6GAL1 with clinical stage and Ki-67 expression. ST6GAL1 expression in tumor tissues positively correlated with clinical stage based on clinical diagnosis (Figure. 1D) and with Ki-67 expression as determined by IHC analysis (Figure 1E). ST6GAL1 is the predominant enzyme that adds α-2,6-linkages of sialic acid to N-glycosylated proteins (17). Therefore, we tested total sialylation levels and detected increased sialylation in tumor samples (Figure 1F and G), which was similar to the effect observed for ST6GAL1 protein expression levels. Furthermore, *in situ* HE and IHC data revealed higher ST6GAL1

expression in the tumor region than in the adjacent normal region (Figure 1H and I). Additionally, it is well known that B72.3 recognizes TAG-72, often carrying sialyl-Tn epitopes. Therefore, we detected expression of B72.3, which is used to detect the expression of tumor-associated sialic acid antigens in tumor tissues (23). B72.3 was significantly higher expression in the tumor samples (Figure 1J). These data indicate that ST6GAL1 and α-2,6-sialylation are significantly upregulated in CRC.

ST6GAL1 promotes CRC cell tumorigenesis and chemoresistance

To dissect the effect of ST6GAL1 expression on CRC tumor cells, we employed a genetic method to establish ST6GAL1-OE or ST6GAL1-KD tumor cell lines. Analysis of the basic expression levels of ST6GAL1 in CRC tumor cell lines showed that the Caco2 cell line highly expressed ST6GAL1 whereas the SW48 cell line endogenously lacked it (Figure S1A and B). ST6GAL1 was overexpressed in SW48 cells but was knocked down in Caco2 cells (Figure S1C and D). As expected, confocal microscopy revealed that SW48 cells lacked endogenous sialylation, which was greatly increased after ST6GAL1 overexpression (Figure S1E). Conversely, ST6GAL1 knockdown in Caco2 cells decreased the sialylation levels (Figure S1F). These were consistent with the WB results (Figure S1G). Interestingly, ST6GAL1 overexpression in SW48 cells significantly increased cell proliferation and colony formation (Figure 2A and B), which decreased upon ST6GAL1 knockdown in Caco2 cells (Figure 2C and D). Importantly, wound healing was significantly improved by ST6GAL1 overexpression in SW48 cells but was modest but significant decrease by ST6GAL1 knockdown in Caco2 cells (Figure 2E). Additionally, upon treatment with 5-FU, fewer AV^+ and 7-AAD^+ cells were detected in the SW48-OE group than in the SW48-EV group (Figure 2F). Compared with the Caco2-EV group, the Caco2-KD group had more AV^+7-AAD^+ cells after 5-FU treatment (Figure 2G). These data confirm that high ST6GAL1 expression promotes CRC progression and chemotherapy resistance.

ST6GAL1 globally enhances the expression of protumor-associated genes

To systematically investigate the transcriptome programs related to ST6GAL1 and CRC progression, we performed RNA-seq for SW48-EV vs. SW48-OE and Caco2-EV vs. Caco2-KD bulk tumor cells (original data shown in Supplementary Tables 3-4). Overall, 3,354 genes were upregulated and 3,088 genes were downregulated in the SW48-EV vs. SW48-OE comparison (Figure S2A), whereas 2,214 genes were upregulated and 1,982 genes were downregulated in the Caco2-EV vs. Caco2-KD comparison (Figure S2A). RNA-seq confirmed a 16-fold upregulation of ST6GAL1 in SW48-OE cells (Figure 3A) and a 4-fold

downregulation in Caco2-KD cells (Figure S2B). A volcano plot revealed that cell proliferation-related genes, such as insulin-like growth factor 2 mRNA binding protein 1 and branched chain amino acid transaminase 1, were greatly upregulated in the SW48-OE group compared with the SW48-EV group (Figure 3A). Cell cycle-related genes, such as cyclin-dependent kinase inhibitor 2A (CDKN2A) and cyclin-dependent kinase-like 2, were upregulated following ST6GAL1 overexpression (Figure 3A). Many cell migration- and motility-related genes were significantly upregulated in the SW48-OE group (Figure 3A). A heatmap revealed globally increased genes in the four modules, including those related to proliferation/cell cycle, migration, motility, and EMT (Figure 3B and Supplementary Table 3). Interestingly, many of the genes related to these four modules were significantly downregulated in the Caco2-KD group compared with the Caco2-EV group (Figure 3B and Supplementary Table 4). We further verified the transcription levels of related genes and found that tumor-promoting genes were upregulated after ST6GAL1 overexpression in SW48 cells but downregulated after ST6GAL1 knockdown in Caco2 cells (Figure 3C and Figure S2C and D). These results suggest that ST6GAL1 promotes tumor growth by regulating proliferation, migration, EMT, and other signaling pathways. Consistently, GO analysis revealed that ST6GAL1 overexpression in SW48 cells was positively related to tumor cell wound healing, proliferation, and adhesion, and the mesenchymal cell differentiation pathway (Figure 3D). Furthermore, gene set enrichment analysis (GSEA) identified regulatory gene sets involved in the response to growth factors, cell junction adhesion/assembly, and stem cell differentiation in ST6GAL1-overexpressing SW48 cells (Figure 3E and Figure S2E). Additionally, angiogenesis, negative regulation of cell death, and the cell surface receptor signaling pathway were involved in cell–cell signaling in SW48-OE cells (Figure 3E and Figure S2E). However, negative regulation of cell adhesion and motility gene sets and other cell proliferation-associated signaling pathways were enriched in ST6GAL1-knockdown Caco2 cells (Figure 3F and Figure S2F). These data suggest that ST6GAL1 transcriptionally reprograms tumor cells to proliferate and migrate.

The multi-omics landscape of N-glycosylation reveals the protumor activity of sialylation in CRC cells after ST6GAL1 overexpression

Previous studies have shown that ST6GAL1-induced protein sialylation is involved in tumor cell proliferation, chemoresistance, and tumorigenesis (24). However, a system-wide view of ST6GAL1-induced sialylation in CRC cells is lacking. Therefore, we employed an unbiased N-glycoproteomic approach in ST6GAL1-overexpressing SW48 cells (original quantitative proteomics and N-glycopeptide modification omics data are shown in Supplementary Tables

5-6). Overall, we identified 2,316 intact glycopeptides that mapped to 687 unique N-glycosites on 398 glycoproteins (Figure S3A and B and Supplementary Table 6). Although the majority (79.48% [546/687]) of unique N-glycosites were annotated as glycosites in the UniProt database (Figure S3B), fewer than half have been reported in the literature, at least 200 of which were assigned via ‘sequence analysis’ (Figure S3C). Although most glycoproteins were extracellular (45.83%) or plasma membrane (26.04%) proteins, nearly 30.00% were intracellular (Figure S3D). These data highlight that many N-glycosites and their functions, particularly those located intracellularly, warrant investigation. Approximately 63.03% (433/687) of glycosites were modified by more than one glycan (Figure S3E) and approximately 32.41% (129/398) of the proteins contained more than one glycosite available for modification (Figure S3F). A heatmap of glycan co-occurrence data showed that glycan pairs among the five glycans (paucimannose, high-mannose, complex/hybrid, fucosylated, and sialylated) co-occurred at the same site, indicating site-specific microheterogeneity and functional complexity of the glycans (Figure S3G).

Compared with the SW48-EV group, 218 intact glycopeptides (IGPs), 87 glycosylated proteins, and 134 glycosylated sites were increased in the SW48-OE group (Figure S4A). An unbiased interrogation of GO-based enrichment terms was performed to gain a global perspective on the effects of ST6GAL1 overexpression. The Ingenuity Pathway Analysis of biological processes (BPs) revealed a strong overrepresentation of several GO terms related to ‘sterol import’ and ‘intestinal cholesterol absorption’ in fucosylated samples, ‘histone lysine methylation’ and ‘negative regulation of protein oligomerization’ in paucimannose samples, and ‘receptor-mediated endocytosis’ and ‘ubiquitin-dependent ERAD pathway’ in high-mannose samples (Figure S4B), which did not explain this phenomenon. Since no sialylation data is available in the proteomics database for analysis, we separated these sialylated proteins to perform enrichment analysis of BP and found that sialylation was markedly positively associated with tumor cell migration, wound healing, and adhesion (Figure 4A). Enrichment analysis also revealed a strong overrepresentation of several GO terms related to ‘regulation of phosphorylation’, which may further regulate receptor activity, such as ‘growth factor activity’ and ‘signaling receptor activity,’ which were identified in an unbiased manner (Figure 4B). Therefore, we distributed the significantly increased sialylated proteins via a heatmap in both the SW48-EV and SW48-OE groups (Figure 4C). The sialylation of many proteins changed, confirming the sialylation function of ST6GAL1 and demonstrating its global influence on cells. Consistently, our omics data revealed that LAMP1 is an ST6GAL1 substrate (Figure 4C),

and the α-2-6 sialylation of LAMP1 has been shown to promote cancer cell invasion and metastasis (25). Sialylation of solute carrier family 3 member 2 (SLC3A2), solute carrier family 2 member 1, and integrin subunit β1 (ITGB1) has also been reported (26, 27). We also identified new substrates of ST6GAL1, such as cell adhesion proteins (LGALS3BP, ATPase Na^+/K^+ transporting subunit β-3, and transmembrane protein 87A) and ferroptosis-related proteins. We explored the associations between these molecules and the survival of patients with CRC in TCGA database and found that their higher expression was associated with a worse prognosis (Figure 4D and Figure S4C). Taken together, these data suggest that sialylation of CRC cells promotes chemoresistance and tumorigenesis.

LGALS3BP sialylation promotes the malignant progression of ST6GAL1-overexpressing CRC cells

LGALS3BP is involved in the growth and progression of many cancer types, and its protumor activity is related mainly to its secreted form, which requires N-glycosylation (28, 29). We first verified the changes in LGALS3BP protein levels between tumor tissues and paired normal tissues via WB. LGALS3BP protein expression was significantly higher in tumor tissues than in normal tissues (Figure 5A and B and Figure S5A). Unexpectedly, the expression level of LGALS3BP significantly increased after ST6GAL1 overexpression in SW48 cells (Figure S5B). Consistently, the IFC data revealed that LGALS3BP expression was higher in the SW48-OE group and co-localized with SNA (Figure S5C). Subsequently, we knocked down LGALS3BP expression in ST6GAL1-overexpressing SW48 cells. WB and IFC revealed that LGALS3BP expression significantly decreased after its knockdown in ST6GAL1-overexpressing SW48 cells (Figure 5C and D). Importantly, the ability of ST6GAL1 to promote tumor cell proliferation and migration and colony formation was significantly blocked after LGALS3BP knockdown in SW48-OE cells (Figure 5E-G and Figure S5D). Furthermore, the chemotherapeutic resistance of SW48-OE cells to 5-FU was blocked by LGALS3BP knockdown (Figure 5H). Therefore, we confirmed that knockdown of LGALS3BP, a substrate of ST6GAL1, can block the protumor function of ST6GAL1 in CRC.

Removal of sialylation blocks the effects of ST6GAL1 on CRC cells

To confirm the effects of ST6GAL1-induced sialylation on CRC cells, we treated SW48-OE and Caco2-EV cells with sialidase (NAs), which significantly decreased sialylation in SW48-OE and Caco2-EV cells, as revealed by a decrease in SNA lectin and IFC staining (Figure 6A, B and Figure S6A). After NA treatment, the ability of ST6GAL1 to promote tumor cell proliferation, migration, and colony formation was significantly blocked (Figure 6C-E). The

resistance effects of ST6GAL1 overexpression against 5-FU chemotherapy were also blocked by desialylation with NA (Figure 6F). Moreover, tumor cell proliferation, migration, and colony formation greatly decreased when Caco2-EV cells were treated with NA (Figure S6B-D). Similarly, desialylation with NA decreased chemoresistance in Caco2-EV-treated cells (Figure 6G). These data indicate that the protumor function of ST6GAL1 occurs mainly through substrate sialylation.

DISCUSSION

In addition to increasing protein stability and diversity in normal tissues, sialylation is critical for a wide variety of biochemical and physiological activities in eukaryotic cells. However, aberrant sialylation and elevated ST6GAL1 expression are increasingly being recognized as features of CRC and many other cancer types (18). Moreover, many sialylated proteins such as PSA, CA125 and thyroglobulin, are clinically used to monitor cancer progression and recurrence (6). However, the substrates of sialylation and the functions of sialyltransferases in cancer cells remain largely unexplored as potential biomarkers or therapeutic targets. In this study, we confirmed that sialylation and ST6GAL1 were upregulated in CRC. *In vitro* data revealed that increased ST6GAL1 expression promoted CRC cell proliferation, migration, and chemoresistance, which was further confirmed by transcriptomic and glycosylated modification sequencing data. Moreover, the removal of sialylation completely blocked the protumor activity of ST6GAL1, demonstrating the importance of sialylation in cancer cells.

To investigate the protumor activity of ST6GAL1 globally, we performed transcriptomic sequencing after ST6GAL1 overexpression and found that many genes related to EMT, proliferation, migration, and metastasis of cancer cells were upregulated. Nidogen 1 (NID1), a component of the extracellular matrix and basement membrane, can link cells to laminins, collagens, and proteoglycans to activate cell EMT and control cancer cell polarization, migration, and invasion (30, 31). Our data revealed that NID1 expression was higher in cell lines with high ST6GAL1 expression. Interestingly, ST6GAL1 overexpression in SW48 cells greatly enhanced the expression of NID1, which was significantly decreased in ST6GAL1-knockdown Caco2 cells. Similarly, the sex-determining region Y-box protein 5-Twist family BHLH transcription factor 1 signal, a master regulator that activates EMT in prostate cancer (32) and gastric cancer (33), was significantly upregulated in SW48 cells overexpressing ST6GAL1. In addition, cyclin-related genes such as CDKN2A were significantly upregulated in ST6GAL1-overexpressing SW48 cells, whereas several cyclin-related genes including cell

division cycle 45, cyclin b2, cyclin-dependent kinase inhibitor 3, and cyclin a2 were downregulated in Caco2-KD cells. Other molecules that promote tumor cell adhesion and metastasis, such as integrin subunits β 4 and 8 (34, 35), were upregulated in ST6GAL1-overexpressing SW48 cells, while integrin subunits α 1 and 2 were downregulated in ST6GAL1-knockdown Caco2 cells. Growth factor-related transcription factors such as the MYC proto-oncogene, an important transcription factor that regulates the occurrence and malignant progression of tumors (36), were significantly downregulated in ST6GAL1-knockdown Caco2 cells. These global changes in the expression of related genes are consistent with the protumor activity of ST6GAL1.

As an important sialyltransferase, the protumor activity of ST6GAL1 may mainly rely on substrate sialylation. Therefore, we performed an N-glycoproteome analysis after ST6GAL1 overexpression to globally view the sialylated substrates and examined the relationship between sialylation and the protumor activity of ST6GAL1. Upon ST6GAL1overexpression, many pathways associated with protumor activities, such as wound healing and proliferation, were enriched in sialylated substrates. Furthermore, ITGB1 sialylation has been reported to increase chemoresistance in tumor cells (10, 11, 37). Many new substrates, such as LGALS3BP (38), ITGB8 (39), CD36 (40) and endothelin-converting enzyme 1 (41), may also participate in malignant tumor progression. LGALS3BP, a family of β-galactoside-binding proteins implicated in cell–cell and cell–matrix interactions, has been found to be modified by terminal sialic acids and fucose (42-44). High LGALS3BP expression in many types of tumors is associated with unfavorable clinical outcomes. Its protumor activity is mainly related to its secreted form, which requires N-glycosylation (29, 45). Surprisingly, our data revealed that LGALS3BP is a direct sialylation substrate of ST6GAL1, which may partially explain the latter's protumor activity. Importantly, the proliferation, invasion, and chemoresistance of ST6GAL1-overexpressing cells were significantly blocked by LGALS3BP knockdown. The migration of SW48 cells increased after ST6GAL1 overexpression, which further confirmed that sialylation of LGALS3BP is important for regulating the migratory behavior of tumor cells. Therefore, further studies should focus on the function and mechanisms of sialylation and sialylated molecules which may lead to the identification of new therapeutic targets. In summary, ST6GAL1 and its sialylated substrates are drawing increasing attention for their clinical value and prospects.

The underlying mechanisms affecting the malignant biological behavior of tumors are complex and diverse. Sialylation is associated with malignant transformations. However, other

molecules in the sialidase family, such as ST6 β-galactoside α2,6-sialyltransferase 2, and ST3 β-galactoside α2,3-sialyltransferase 4, regulate sialylation, and their contribution to the regulation of sialylation cannot be ruled out. Our omics results revealed that some molecules do not undergo sialylation themselves, but that sialylation occurs after ST6GAL1 overexpression. Therefore, sialic acid modification caused by ST6GAL1 affects tumor cell function. Combined with the *in vitro* results, we showed that ST6GAL1 upregulation was associated with more significant malignant characteristics, such as tumor proliferation and migration. Therefore, ST6GAL1 may increase the aggressiveness of tumor cells. Despite *in vitro* experiments and omics results, ST6GAL1, LGALS3BP and sialylation are valuable targets for clinical treatment of CRC. However, due to the lack of *in vivo* experimental verification, future studies may need to focus more on *in vivo* experiments of these targets. Totally speaking, the influence of other members of the sialic acid family on the biological behavior of tumor cells warrants further exploration.

CONCLUSION

This study identified a novel mechanism by which ST6GAL1 promotes CRC. It shows that ST6GAL1 promotes CRC progression through LGALS3BP sialylation, and up-regulation of protumor genes promotes CRC tumorigenesis and chemoresistance. It provides an important perspective and new direction for the future treatment of CRC.

Acknowledgments: We would like to thank all the research staff who made it possible to perform this study.

Conflicts of interest: Authors declare no conflicts of interest.

Funding: This study was supported by the Natural Science Foundation of China (grant numbers 82373404 and 32100707).

Data availability: Data will be made available on reasonable request.

Submitted: 12 November 2024

Accepted: 31 January 2025

Published online:

REFERENCES

1. Siegel RL, Kratzer TB, Giaquinto AN, Sung H, Jemal A. Cancer statistics, 2025. CA Cancer J Clin. 2025.
2. Spaander MCW, Zauber AG, Syngal S, Blaser MJ, Sung JJ, You YN, et al. Young-onset colorectal cancer. Nature Reviews Disease Primers. 2023;9(1).
3. Siegel RL, Wagle NS, Cercek A, Smith RA, Jemal A. Colorectal cancer statistics, 2023. CA: A Cancer Journal for Clinicians. 2023;73(3):233-54.
4. Li F, Ding J. Sialylation is involved in cell fate decision during development, reprogramming and cancer progression. Protein & Cell. 2018;10(8):550-65.
5. Dall'Olio F, Chiricolo M, Ceccarelli C, Minni F, Marrano D, Santini D. β-galactoside α2,6 sialyltransferase in human colon cancer: contribution of multiple transcripts to regulation of enzyme activity and reactivity withsambucus nigra agglutinin. International journal of cancer. 2000;88(1):58-65.
6. Badr HA, AlSadek DMM, Darwish AA, ElSayed AI, Bekmanov BO, Khussainova EM, et al. Lectin approaches for glycoproteomics in FDA-approved cancer biomarkers. Expert Review of Proteomics. 2014;11(2):227-36.
7. Lu J, Isaji T, Im S, Fukuda T, Hashii N, Takakura D, et al. β-Galactoside α2,6-Sialyltranferase 1 Promotes Transforming Growth Factor-β-mediated Epithelial-Mesenchymal Transition. Journal of Biological Chemistry. 2014;289(50):34627-41.
8. Britain CM, Bhalerao N, Silva AD, Chakraborty A, Buchsbaum DJ, Crowley MR, et al. Glycosyltransferase ST6Gal-I promotes the epithelial to mesenchymal transition in pancreatic cancer cells. Journal of Biological Chemistry. 2021;296.
9. Hugonnet M, Singh P, Haas Q, von Gunten S. The Distinct Roles of Sialyltransferases in Cancer Biology and Onco-Immunology. Frontiers in immunology. 2021;12.
10. Swindall AF, Bellis SL. Sialylation of the Fas Death Receptor by ST6Gal-I Provides Protection against Fas-mediated Apoptosis in Colon Carcinoma Cells. Journal of Biological Chemistry. 2011;286(26):22982-90.
11. Zhuo Y, Chammas R, Bellis SL. Sialylation of 1 Integrins Blocks Cell Adhesion to Galectin-3 and Protects Cells against Galectin-3-induced Apoptosis. Journal of Biological Chemistry. 2008;283(32):22177-85.
12. Holdbrooks AT, Britain CM, Bellis SL. ST6Gal-I sialyltransferase promotes tumor necrosis factor (TNF)-mediated cancer cell survival via sialylation of the TNF receptor 1 (TNFR1) death receptor. Journal of Biological Chemistry. 2018;293(5):1610-22.
13. Swindall AF, Londoño-Joshi AI, Schultz MJ, Fineberg N, Buchsbaum DJ, Bellis SL. ST6Gal-I Protein Expression Is Upregulated in Human Epithelial Tumors and Correlates with Stem Cell Markers in Normal Tissues and Colon Cancer Cell Lines. Cancer research. 2013;73(7):2368-78.
14. Schultz MJ, Holdbrooks AT, Chakraborty A, Grizzle WE, Landen CN, Buchsbaum DJ, et al. The Tumor-Associated Glycosyltransferase ST6Gal-I Regulates Stem Cell Transcription Factors and Confers a Cancer Stem Cell Phenotype. Cancer research. 2016;76(13):3978-88.
15. Cui H, Yang S, Jiang Y, Li C, Zhao Y, Shi Y, et al. The glycosyltransferase ST6Gal-I is enriched in cancer stem-like cells in colorectal carcinoma and contributes to their chemo-resistance. Clinical and Translational Oncology. 2018;20(9):1175-84.
16. Lau JTY, Marathe H, Manhardt CT, Irons EE, Punch PR. The sialyltransferase ST6GAL1 protects against radiation-induced gastrointestinal damage. Glycobiology. 2020;30(7):446-53.
17. Dall'Olio F. The sialyl-alpha2,6-lactosaminyl-structure: biosynthesis and functional role. Glycoconj J. 2000;17(10):669-76.
18. Garnham R, Scott E, Livermore K, Munkley J. ST6GAL1: A key player in cancer (Review). Oncology Letters. 2019.
19. Britain CM, Holdbrooks AT, Anderson JC, Willey CD, Bellis SL. Sialylation of EGFR by the ST6Gal-I sialyltransferase promotes EGFR activation and resistance to gefitinib-mediated cell death. Journal of Ovarian Research. 2018;11(1).
20. Machado E, White-Gilbertson S, van de Vlekkert D, Janke L, Moshiach S, Campos Y, et al. Regulated lysosomal exocytosis mediates cancer progression. Science advances. 2015;1(11):e1500603.
21. Jones RB, Dorsett KA, Hjelmeland AB, Bellis SL. The ST6Gal-I sialyltransferase protects tumor cells against hypoxia by enhancing HIF-1α signaling. Journal of Biological Chemistry. 2018;293(15):5659-67.
22. Li L, Qin S, Tan H, Zhou J. LGALS3BP is a novel and potential biomarker in clear cell renal cell carcinoma. Aging (Albany NY). 2024;16(4):4033-51.
23. Yao Y, Kim G, Shafer S, Chen Z, Kubo S, Ji Y, et al. Mucus sialylation determines intestinal host-commensal homeostasis. Cell. 2022;185(7):1172-88.e28.
24. Garnham R, Scott E, Livermore KE, Munkley J. ST6GAL1: A key player in cancer. Oncol Lett. 2019;18(2):983-9.
25. Wang Q, Yao J, Jin Q, Wang X, Zhu H, Huang F, et al. LAMP1 expression is associated with poor prognosis in breast cancer. Oncol Lett. 2017;14(4):4729-35.
26. Cotton S, Ferreira D, Soares J, Peixoto A, Relvas-Santos M, Azevedo R, et al. Target Score-A Proteomics

Data Selection Tool Applied to Esophageal Cancer Identifies GLUT1-Sialyl Tn Glycoforms as Biomarkers of Cancer Aggressiveness. Int J Mol Sci. 2021;22(4).
27. Agrawal P, Chen S, de Pablos A, Jame-Chenarboo F, Miera Saenz de Vega E, Darvishian F, et al. Integrated in vivo functional screens and multi-omics analyses identify α-2,3-sialylation as essential for melanoma maintenance. bioRxiv. 2024.
28. Capone E, Iacobelli S, Sala G. Role of galectin 3 binding protein in cancer progression: a potential novel therapeutic target. J Transl Med. 2021;19(1):405.
29. Chen Y, Hojo S, Matsumoto N, Yamamoto K. Regulation of Mac-2BP secretion is mediated by its N-glycan binding to ERGIC-53. Glycobiology. 2013;23(7):904-16.
30. Rokavec M, Jaeckel S, Hermeking H. Nidogen-1/NID1 Function and Regulation during Progression and Metastasis of Colorectal Cancer. Cancers. 2023;15(22).
31. Rokavec M, Bouznad N, Hermeking H. Paracrine Induction of Epithelial-Mesenchymal Transition Between Colorectal Cancer Cells and its Suppression by a p53/miR-192/215/NID1 Axis. Cellular and Molecular Gastroenterology and Hepatology. 2019;7(4):783-802.
32. Hu J, Tian J, Zhu S, Sun L, Yu J, Tian H, et al. Sox5 contributes to prostate cancer metastasis and is a master regulator of TGF-β-induced epithelial mesenchymal transition through controlling Twist1 expression. British Journal of Cancer. 2017;118(1):88-97.
33. You J, Zhao Q, Fan X, Wang J. SOX5 promotes cell invasion and metastasis via activation of Twist-mediated epithelial–mesenchymal transition in gastric cancer . OncoTargets and Therapy. 2019;Volume 12:2465-76.
34. Zhang W, Zhang B, Vu T, Yuan G, Zhang B, Chen X, et al. Molecular characterization of pro-metastatic functions of β4-integrin in colorectal cancer. Oncotarget. 2017;8(54):92333-45.
35. Giancotti FG. Targeting integrin β4 for cancer and anti-angiogenic therapy. Trends in Pharmacological Sciences. 2007;28(10):506-11.
36. Dhanasekaran R, Deutzmann A, Mahauad-Fernandez WD, Hansen AS, Gouw AM, Felsher DW. The MYC oncogene — the grand orchestrator of cancer growth and immune evasion. Nature Reviews Clinical Oncology. 2021;19(1):23-36.
37. Liu J, Dong X, Xie R, Tang Y, Thomas AM, Li S, et al. N-linked α2,6-sialylation of integrin β1 by the sialyltransferase ST6Gal1 promotes cell proliferation and stemness in gestational trophoblastic disease. Placenta. 2024;149:18-28.
38. Stampolidis P, Ullrich A, Iacobelli S. LGALS3BP, lectin galactoside-binding soluble 3 binding protein, promotes oncogenic cellular events impeded by antibody intervention. Oncogene. 2013;34(1):39-52.
39. Qiu S, Qiu Y, Deng L, Nie L, Ge L, Zheng X, et al. Cell softness reveals tumorigenic potential via ITGB8/AKT/glycolysis signaling in a mice model of orthotopic bladder cancer. Chinese medical journal. 2023.
40. Liu L-Z, Wang B, Zhang R, Wu Z, Huang Y, Zhang X, et al. The activated CD36-Src axis promotes lung adenocarcinoma cell proliferation and actin remodeling-involved metastasis in high-fat environment. Cell Death & Disease. 2023;14(8).
41. Chen L, Lu Y, Zhao M, Xu J, Wang Y, Xu Q, et al. A non-canonical role of endothelin converting enzyme 1 (ECE1) in promoting lung cancer development via directly targeting protein kinase B (AKT). The journal of gene medicine. 2023:e3612.
42. Sasaki T, Brakebusch C, Engel J, Timpl R. Mac-2 binding protein is a cell-adhesive protein of the extracellular matrix which self-assembles into ring-like structures and binds beta1 integrins, collagens and fibronectin. Embo j. 1998;17(6):1606-13.
43. Linsley PS, Horn D, Marquardt H, Brown JP, Hellström I, Hellström KE, et al. Identification of a novel serum protein secreted by lung carcinoma cells. Biochemistry. 1986;25(10):2978-86.
44. Loimaranta V, Hepojoki J, Laaksoaho O, Pulliainen AT. Galectin-3-binding protein: A multitask glycoprotein with innate immunity functions in viral and bacterial infections. Journal of leukocyte biology. 2018;104(4):777-86.
45. Capone E, Iacobelli S, Sala G. Role of galectin 3 binding protein in cancer progression: a potential novel therapeutic target. Journal of Translational Medicine. 2021;19(1).

FIGURES WITH LEGENDS

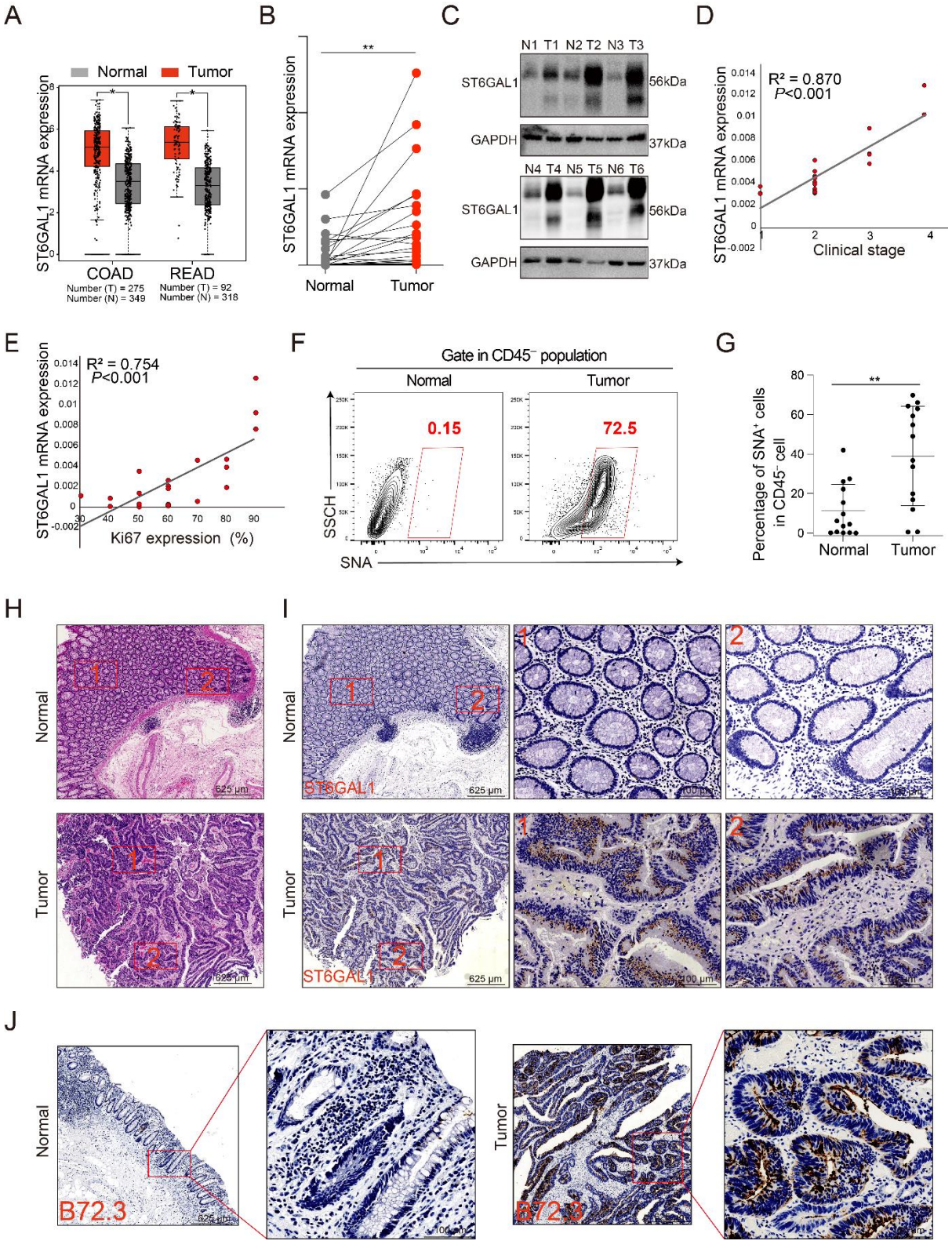

Figure 1. ST6GAL1 expression and sialylation are strongly increased in the tumor tissue of CRC patients. (A) ST6GAL1 mRNA expression data were collected from colon adenocarcinoma (COAD) and rectum adenocarcinoma (READ) patients in the TCGA database. The corresponding normal tissues in the GTEx database were included as controls. The box plot data was supplied. (B) ST6GAL1 mRNA expression was quantified by reverse

transcription-quantitative polymerase chain reaction (RT-qPCR) in fresh tumor tissues compared with normal tissues from twenty-two clinical CRC patients. (C) The protein level of ST6GAL1 was detected in six clinical samples from CRC patients by western blot (WB). (D) Correlation of the ST6GAL1 mRNA level and clinical grade (n=22, Spearman correlation coefficient). (E) Correlation between the ST6GAL1 mRNA level and the Ki-67 level. (n=22; Pearson correlation coefficient). (F) The sialylation level was measured by SNA staining and detected in fresh tumor tissues compared with normal tissue from CRC patients by flow cytometry (n=14). (G) Statistical results of the percentage of SNA-positive tumor cells from Figure F. (H and I) Representative HE staining and IHC staining of ST6GAL1 in tumor tissue and adjacent normal tissue from CRC patients (scale bars, 625 μm; scale bars, 100 μm). (J) Representative HE staining and IHC staining of B72.3 in tumor tissue and adjacent normal tissue from CRC patient (scale bars, 625 μm; scale bars, 100 μm). **P*<0.05, ***P*<0.01, by Student's *t*-test (A, B and G). The data are presented as the mean±SD of three independent experiments.

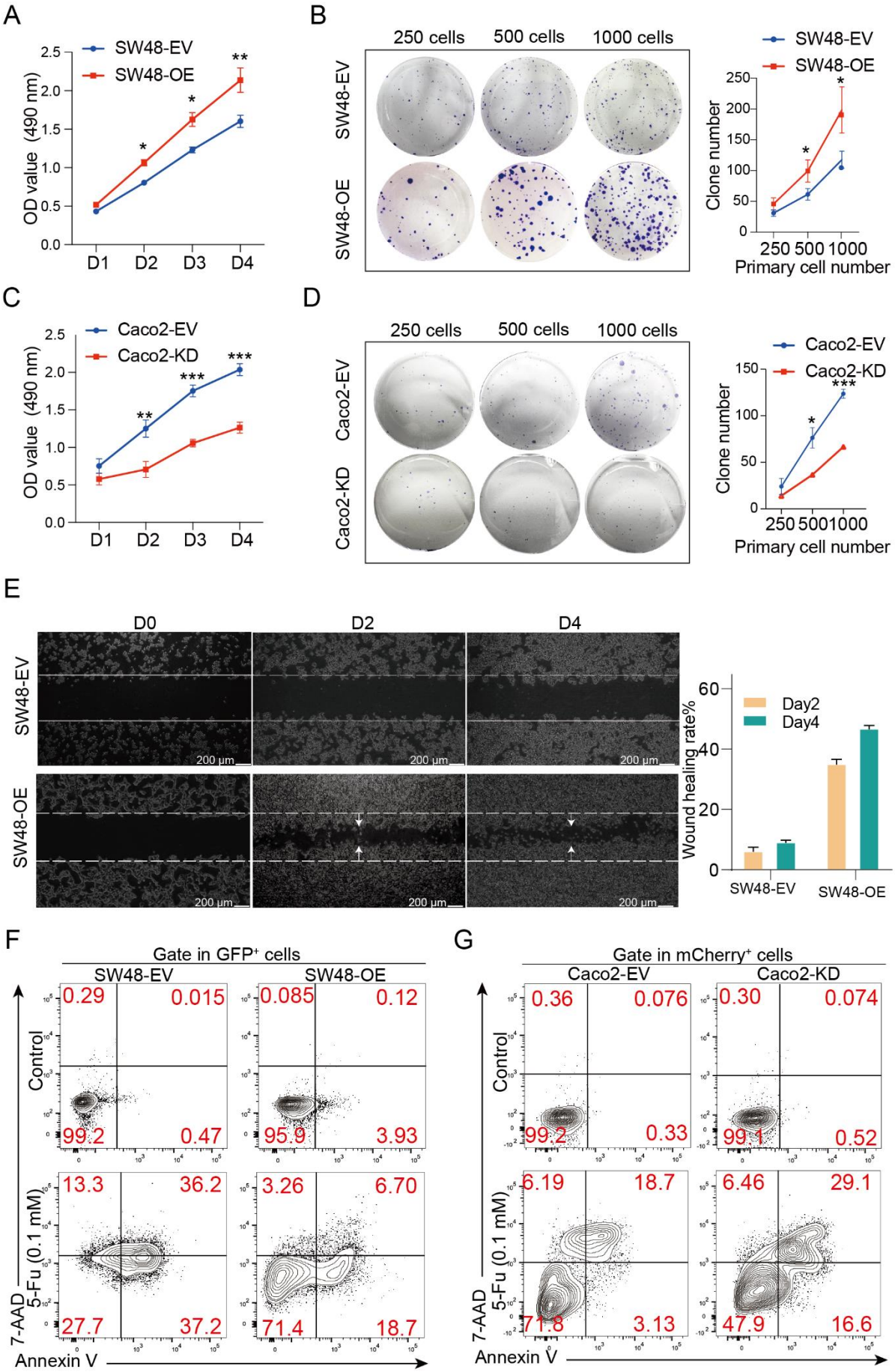
A
SW48-EV
SW48-OE
OD value (490 nm)
D1
D2
D3
D4
B
250 cells
500 cells
1000 cells
SW48-EV
SW48-OE
Clone number
Primary cell number
C
Caco2-EV
Caco2-KD
D
E
D0
D2
D4
200 μm
Wound healing rate%
Day2
Day4
F
Gate in GFP⁺ cells
Control
5-Fu (0.1 mM)
7-AAD
Annexin V
0.29
0.015
99.2
0.47
13.3
36.2
27.7
37.2
0.085
0.12
95.9
3.93
3.26
6.70
71.4
18.7
G
Gate in mCherry⁺ cells
0.36
0.076
99.2
0.33
6.19
18.7
71.8
3.13
0.30
0.074
99.1
0.52
6.46
29.1
47.9
16.6

Figure 2. ST6GAL1 is associated with CRC cell proliferation, migration, and chemoresistance. After constructing the ST6GAL1-overexpressing (OE) SW48 cell line (SW48-OE) and knockdown (KD) Caco2 cell line (Caco2-KD), as well as the related empty virus (EV)-expressing control cell lines SW48-EV and Caco2-EV, tumor cell viability, colony formation and wound healing were tested. (A and C) Tumor cell viability was measured via the MTT assay in SW48 (A) and Caco2 (C) cells. (B and D) Tumor cell colony formation was detected after 14 days of culture, the numbers of clones were counted, and the statistical results are shown. (E) Wound healing assay of the SW48-EV and SW48-OE cell lines on days 0, 2 and 4 (scale bars, 200 μm) and corresponding statistical results. (F and G) Tumor cells were treated with 5-Fu (0.1 mM) or without 5-Fu for 48 hours, and Annexin V and 7-AAD staining was detected by flow cytometry in SW48-EV, SW48-OE, Caco2-EV, and Caco2-KD cell lines. **P*<0.05, ***P*<0.01, ****P*<0.001 by Student's *t*-test (A-D). The data are presented as the mean±SD of three independent experiments.

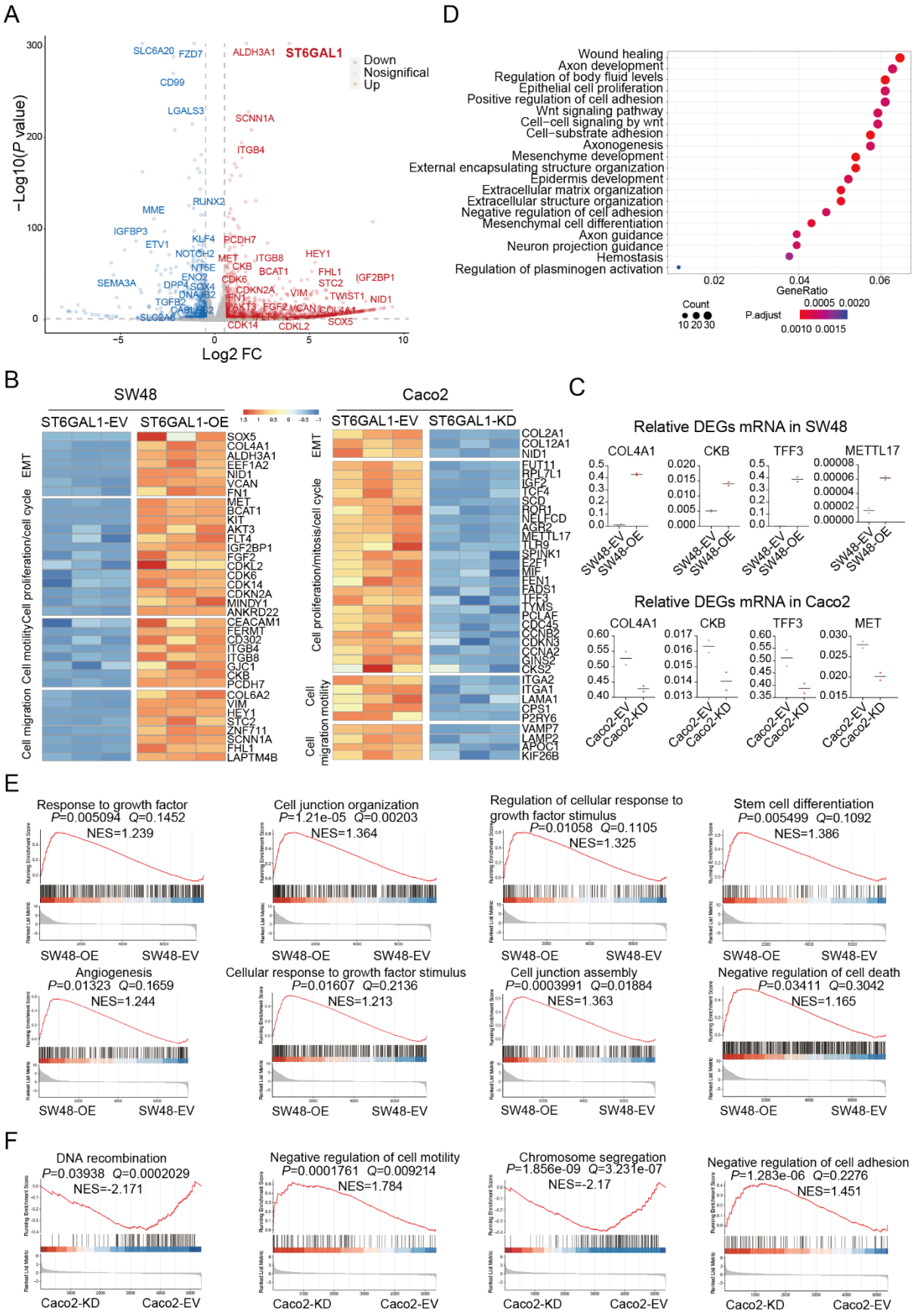

Figure 3. ST6GAL1 expression mediates transcriptome changes in CRC cells. Two cell line

groups, SW48-EV vs. SW48-OE and Caco2-EV vs. Caco2-KD, were subjected to RNA-sequencing (RNA-seq) analysis. (A) Volcano plot showing all genes expressed in the SW48-EV and SW48-OE cell lines. The x-axis shows the $\log_2$ fold change (FC, SW48-OE vs. SW48-EV), and the y-axis shows the $-\log_{10} P$ value, which represents the threshold values in log transformation. Each dot represents a differentially expressed gene (DEG). The red dots indicate significantly upregulated DEGs, the blue dots indicate significantly downregulated DEGs, and the gray dots represent nonsignificant DEGs. (B) Heatmap showing the relative expression of selected genes across ST6GAL1-OEand ST6GAL1-KD cell lines in four different functional modules. (C) The transcription levels of some DEGs were confirmed in ST6GAL1-OE and ST6GAL1-KD cell lines via RT-qPCR. (D) GO enrichment analysis of the SW48-EV vs. SW48-OE cell lines. (E) Gene set enrichment analysis (GSEA) of the SW48-OE cell line revealed an upregulated signaling pathway compared with that of the SW48-EV cell line. NES, normalized enrichment score. (F) GSEA of the Caco2-KD cell line revealed upregulated and downregulated signaling pathways compared with those in the Caco2-EV cell line. The data are presented as the mean±SD of three independent experiments (C). DEGs that had $P<0.05$ and $\log_2$ FC>1 or <-1 (D, B, E and F) were selected.

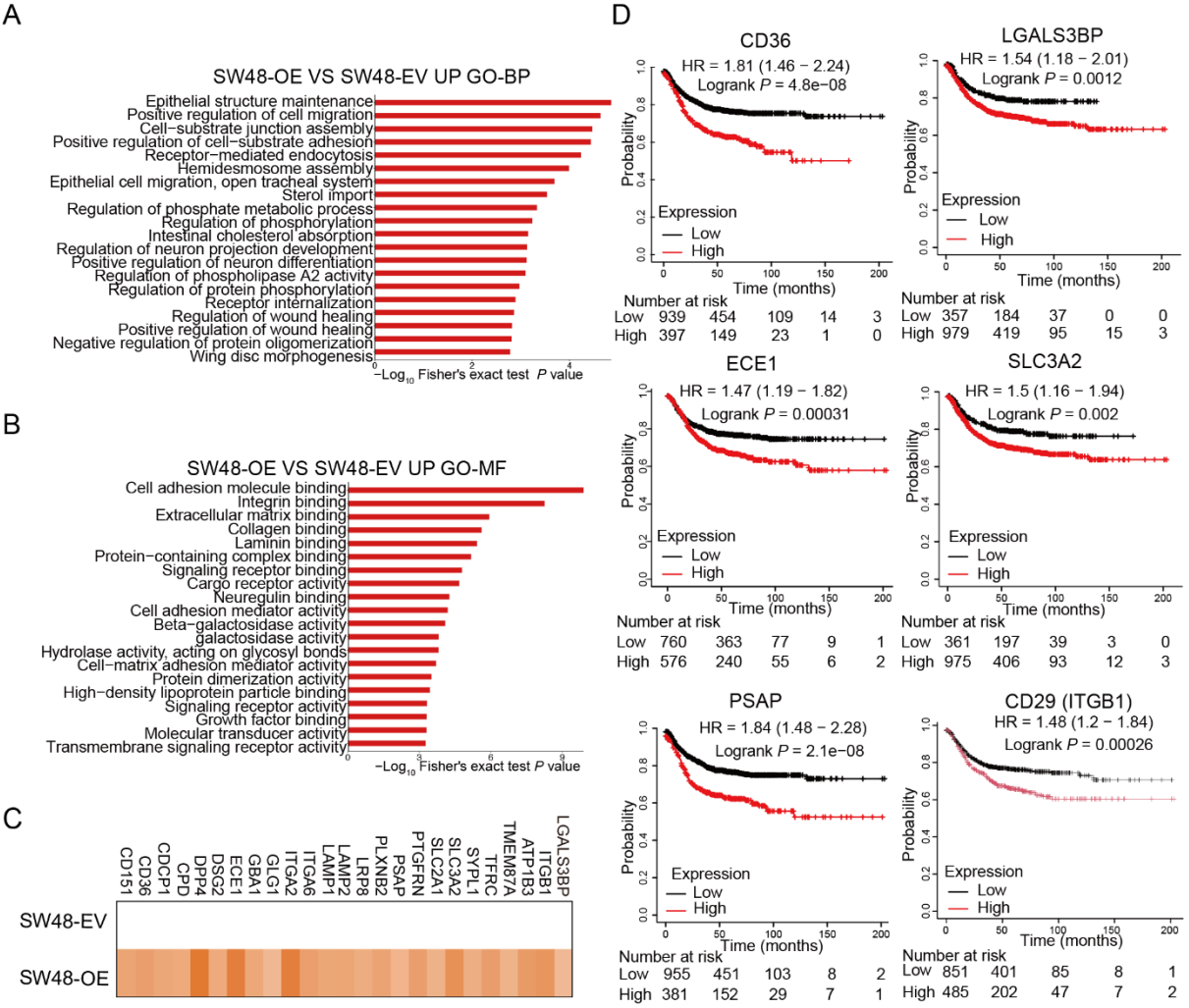

Figure 4. ST6GAL1 increases tumor cell sialylation, and many sialylated substrates are correlated with tumor progression. Modification omics was performed on SW48-EV and SW48-OE cell lines, and sialylation was analyzed. (A) Bar plot of biological process (BP) terms based on the GO enrichment results for sialylation-modified molecules after ST6GAL1 was overexpressed in the SW48 cell line. (Fisher's exact test, $P<0.05$). (B) Bar plot of

molecular function based on GO enrichment results of sialylation-modified molecules after ST6GAL1 was overexpressed in the SW48 cell line. (Fisher's exact test, $P<0.05$). (C) Heatmap of increased sialylation of proteins in SW48-OE cells compared with SW48-EV cells. (D) Survival analysis of molecules with increased sialylation modifications and Kaplan-Meier plotter database analysis using RNA-seq data from the TCGA, EGA, and GEO databases.

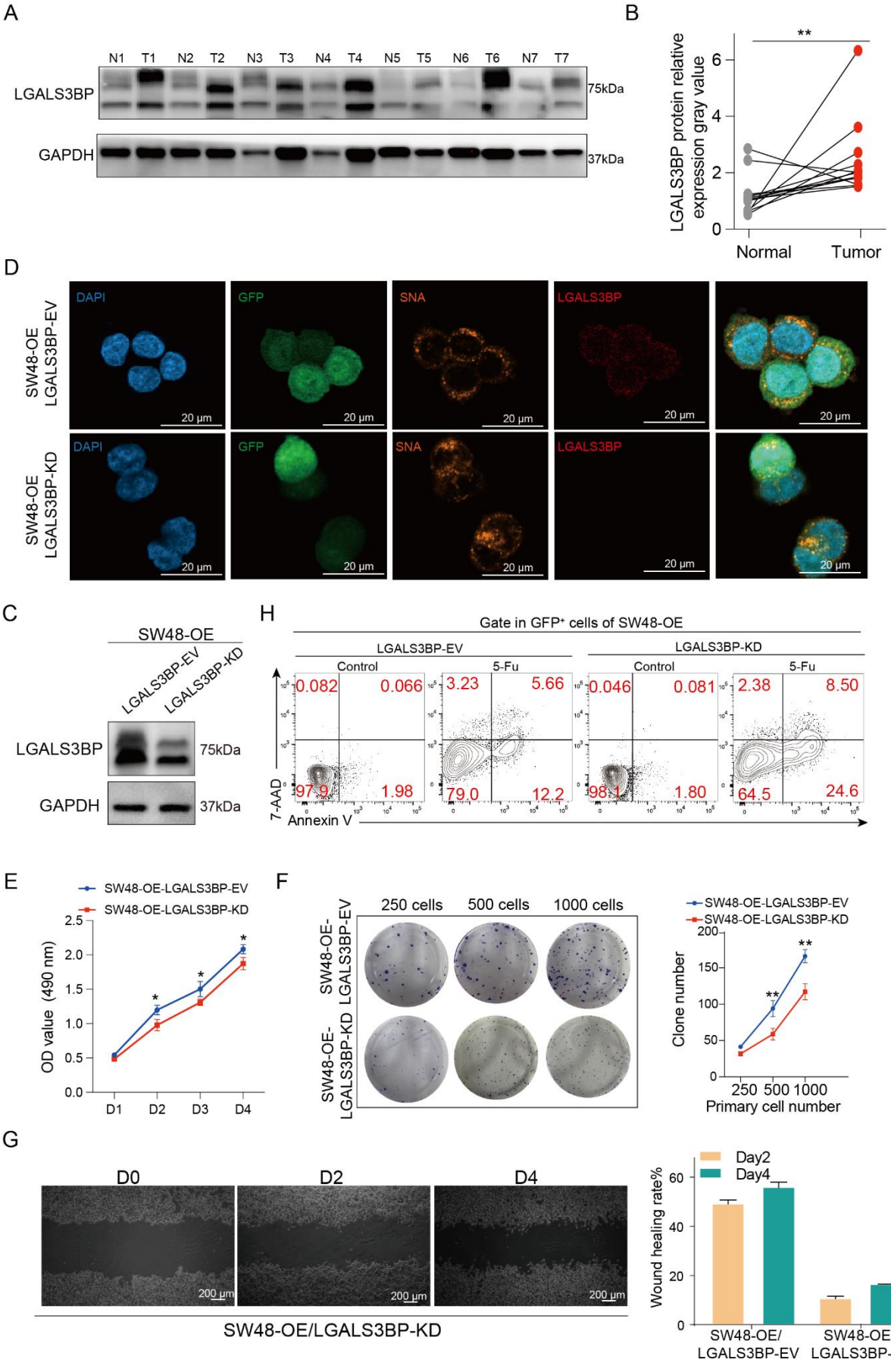
A
N1 T1 N2 T2 N3 T3 N4 T4 N5 T5 N6 T6 N7 T7
LGALS3BP
75kDa
GAPDH
37kDa
B
LGALS3BP protein relative expression gray value
**
Normal
Tumor
D
SW48-OE LGALS3BP-EV
SW48-OE LGALS3BP-KD
DAPI
GFP
SNA
LGALS3BP
20 μm
C
SW48-OE
LGALS3BP-EV
LGALS3BP-KD
LGALS3BP
75kDa
GAPDH
37kDa
H
Gate in GFP+ cells of SW48-OE
LGALS3BP-EV
LGALS3BP-KD
Control
5-Fu
0.082
0.066
97.9
1.98
3.23
5.66
79.0
12.2
0.046
0.081
98.1
1.80
2.38
8.50
64.5
24.6
7-AAD
Annexin V
E
SW48-OE-LGALS3BP-EV
SW48-OE-LGALS3BP-KD
OD value (490 nm)
D1
D2
D3
D4
F
250 cells
500 cells
1000 cells
SW48-OE-LGALS3BP-EV
SW48-OE-LGALS3BP-KD
Clone number
Primary cell number
G
D0
D2
D4
200 μm
SW48-OE/LGALS3BP-KD
Day2
Day4
Wound healing rate%
SW48-OE/LGALS3BP-EV
SW48-OE/LGALS3BP-KD

Figure 5. Sialylation of LGALS3BP promotes the migration of ST6GAL1-OE cells. (A) WB analysis of LGALS3BP protein levels in tumor and paired normal tissues from CRC patients (n=7). (B) Gray value statistical results for CRC patients (n=13). (C) LGALS3BP protein expression in LGALS3BP-EV and LGALS3BP-KD cell lines was quantified by WB. (D) Staining of SNA (orange) and LGALS3BP (red) in the LGALS3BP-EV and LGALS3BP-KD of SW48-OE (GFP, green) cell line by immunofluorescence (IFC). Nuclei were counterstained with DAPI (blue). (scale bars, 20 μm). (E) Tumor cell viability was measured using an MTT assay in LGALS3BP-KD cells. (F) Tumor cell colony formation was detected after 14 days of culture, the number of clones was counted, and the statistical results are shown. (G) Wound healing assay of LGALS3BP-KD in SW48-OE cell line on days 0, 2 and 4 (scale bars, 20 μm) and corresponding statistical results. (H) Tumor cells were treated with or without 5-Fu (0.1 mM) for 48 hours, and Annexin V and 7-AAD staining was detected by flow cytometry in LGALS3BP-EV and LGALS3BP-KD of SW48-OE cell line. **P*<0.05, ***P*<0.01, by Student's *t*-test (B, E and F). The data are presented as the mean±SD of three independent experiments.

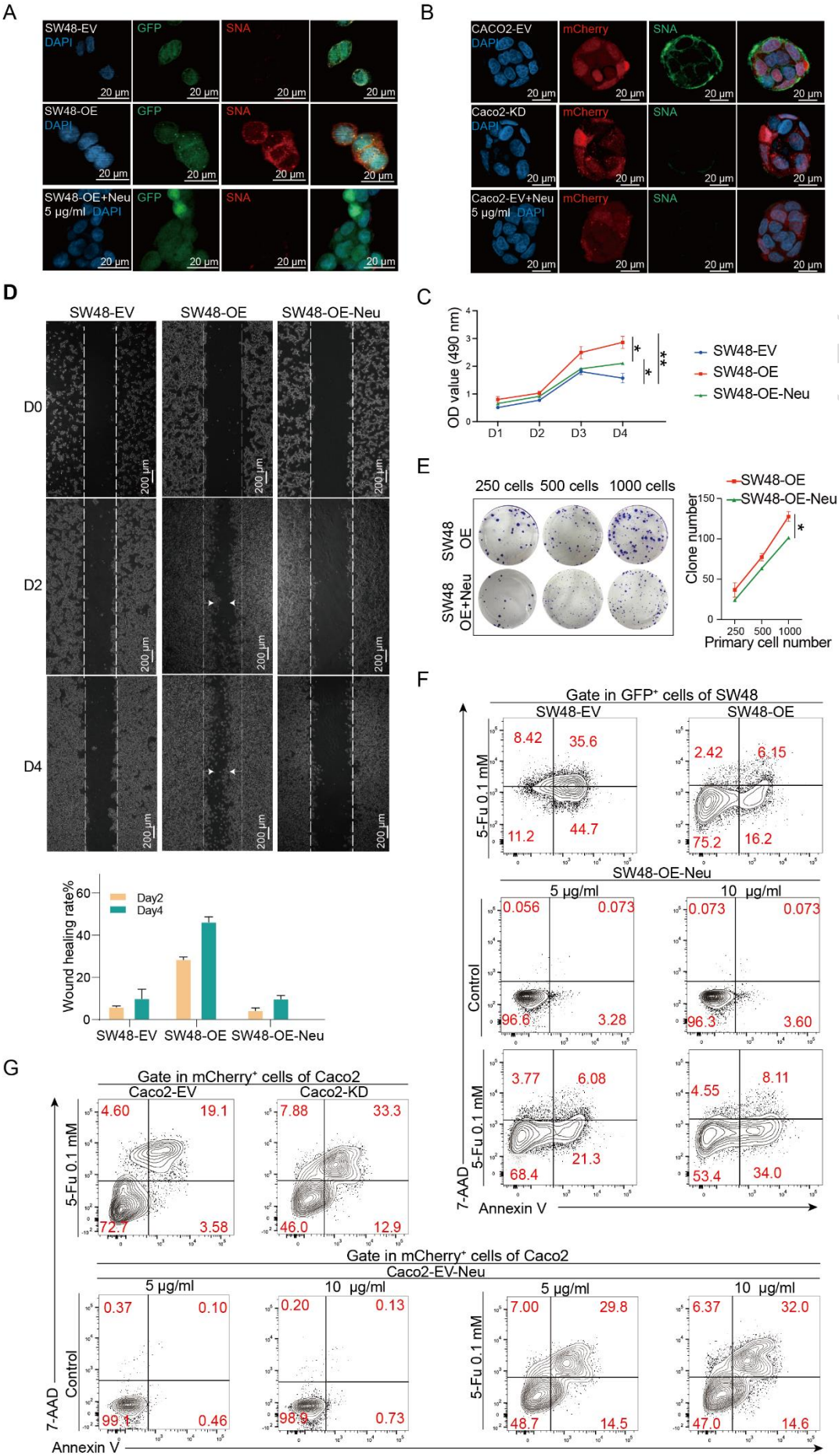
A
SW48-EV
DAPI
GFP
SNA
SW48-OE
SW48-OE+Neu
5 μg/ml
20 μm
B
CACO2-EV
mCherry
Caco2-KD
Caco2-EV+Neu
C
OD value (490 nm)
D1
D2
D3
D4
SW48-EV
SW48-OE
SW48-OE-Neu
D
D0
D2
D4
200 μm
Wound healing rate%
Day2
Day4
E
250 cells 500 cells 1000 cells
SW48 OE
SW48 OE+Neu
Clone number
Primary cell number
F
Gate in GFP⁺ cells of SW48
5-Fu 0.1 mM
Control
7-AAD
Annexin V
8.42
35.6
11.2
44.7
2.42
6.15
75.2
16.2
5 μg/ml
10 μg/ml
0.056
0.073
96.6
3.28
96.3
3.60
3.77
6.08
21.3
68.4
4.55
8.11
53.4
34.0
G
Gate in mCherry⁺ cells of Caco2
4.60
19.1
72.7
3.58
7.88
33.3
46.0
12.9
Caco2-EV-Neu
0.37
0.10
99.1
0.46
0.20
0.13
98.9
0.73
7.00
29.8
48.7
14.5
6.37
32.0
47.0
14.6

Figure 6. Desialylation blocks CRC cell proliferation, migration, and chemoresistance. SW48-EV or Caco2-OE cells were treated with α-(2-3, 6, 8, 9) neuraminidase (NA) for 24 hours at a concentration of 5 μg/ml. (A and B) IFC staining of SNA (red) in SW48-EV (GFP, green) and SW48-OE (GFP, green) and SW48-OE (GFP, green) cell lines treated with NA (5 μg/ml) for 24 hours. Nuclei were counterstained with DAPI (blue) (scale bars, 20 μm). (B) IFC staining of SNA (green) in Caco2-EV (mCherry, red) and Caco2-KD (mCherry, red) cell lines and Caco2-EV (mCherry, red) cell lines treated with NA (5 μg/ml) for 24 hours. Nuclei were counterstained with DAPI (blue). (scale bars, 20 μm). (C) MTT assay results in SW48-OE cells. (D) Wound healing assay of SW48-OE cells on days 0, 2, 4 (scale bars, 200 μm) and corresponding statistical results. (E) Colony formation assay in SW48-OE cells. (F and G) SW48-OE (F) or Caco2-EV (G) cells were treated with or without 5-Fu combined with NA (5 μg/ml and 10 μg/ml) for 48 hours, after which Annexin V and 7-AAD staining was detected via flow cytometry. **P*<0.05, ***P*<0.01, by Student's *t*-test (C and E). The data are presented as the mean±SD of three independent experiments.

SUPPLEMENTAL DATA

Supplemental data are available at the following link:
https://www.bjbms.org/ojs/index.php/bjbms/article/view/11663/3738